44th AIAA/ASME/ASCE/AHS Structures, Structural Dynamics, and Materials Confere
7-10 April 2003, Norfolk, Virginia

AIAA 2003-1691

A NEW LAGRANGIAN-EULERIAN SHELL-FLUID COUPLING ALGORITHM BASED ON LEVEL SETS

Fehmi Cirak*
Center for Advanced Computing Research
California Institute of Technology
Pasadena, CA 91125

Raúl Radovitzky†
Department of Aeronautics and Astronautics
Massachusetts Institute of Technology
Cambridge, MA 02139

We propose a computational method for the coupled simulation of a compressible flow interacting with a thin-shell structure undergoing large deformations. An Eulerian finite volume formulation is adopted for the fluid and a Lagrangian formulation based on subdivision finite elements is adopted for the shell response. The coupling between the fluid and the solid response is achieved via a novel approach based on level sets. The basic approach furnishes a general algorithm for coupling Lagrangian shell solvers with Cartesian grid based Eulerian fluid solvers. The efficiency and robustness of the proposed approach is demonstrated with an airbag deployment simulation. It bears emphasis that in the proposed approach the solid and the fluid components as well as their coupled interaction are considered in full detail and modeled with an equivalent level of fidelity without any oversimplifying assumptions or bias towards a particular physical aspect of the problem.

Introduction

A large class of fluid-shell interaction problems requires a combined Lagrangian/Eulerian description of the governing dynamics. Lagrangian formulations are inadequate for describing high-speed flows and/or flows with significant vorticity because the mesh inevitably incurs deformation-induced distortions, which breaks the numerical method. This problem can be alleviated by recourse to continuous adaptive remeshing,[1] but not cured in general, especially in three dimensions. Eulerian approaches with the field equations formulated in terms of spatial variables and fixed meshes are better suited for most fluid flows. By contrast, large deformations of solids are more adequately described in a Lagrangian framework. The principal advantage of the Lagrangian approach for solids lies in its ability to naturally track the evolution of material properties associated with the material points as well as in the treatment of boundary conditions at material surfaces such as free boundaries or fluid-solid interfaces. In contrast to Eulerian approaches, boundary conditions are enforced at material surfaces *ab initio* and require no special attention. In this work, we adopt an Eulerian finite volume formulation for the fluid and a Lagrangian formulation based on subdivision finite elements for the shell.

A number of different basic strategies have been proposed for coupling the response of interacting solids and fluids. In the conventional Arbitrary-Lagrangian-Eulerian (ALE) approach,[2] the coupling of the fixed Eulerian and moving Lagrangian meshes is accomplished through an intermediate region in which the mesh moves with a prescribed velocity. The specification of the mesh evolution is key to the success of ALE methods, which unfortunately requires a priori knowledge of the solution. In particular, for structures with very large deformations the success of ALE methods is not always assured. The ALE method also requires frequent mesh updating as the solid boundary undergoes large deformations.

Our approach has its origin in the Ghost Fluid Method[3] and is an extension of the general Eulerian-Lagrangian coupling strategy for bulk solids with compressible flows presented previously.[4,5] The dynamic deformations of the solid shell are formulated within a large-deformation Lagrangian finite element framework and an Eulerian finite volume formulation is adopted for solving the compressible flow equations. The coupling between the Eulerian fluid solver and the Lagrangian shell solver is accomplished *via* a novel technique based on level sets. At each time step, the signed distance function from the solid boundary is computed on the Eulerian grid by a demonstrably optimal algorithm proposed by Mauch.[6] The resulting implicit representation of the fluid-shell boundary in the deformed configuration is used to enforce the conservation laws at the boundary between the fluid and the solid. It bears emphasis that the ability to compute the level set with optimal complexity prevents this step from becoming a computational bottleneck in the simulations.

In the following sections, we first describe the numerical formulations employed for the shell and the fluid. Subsequently, we describe the fluid-shell coupling algorithm. Finally, we present an example of application of the overall numerical method to the simulation of airbag deployment. This example demonstrates the feasibility and power of the proposed computational strategy in capturing the intricate features of the interaction between the flow and the shell.

Lagrangian Thin-Shell Solver

The mechanical shell response is computed with the recently introduced subdivision finite elements.[7,8] We employ a Kirchhoff-Love type kinematic assumption, which allows for arbitrary large displacements and rotations of the shell. As it is well known, the Kirchhoff-Love energy functional of the thin-shell depends on the first and second order derivatives of displacements. It is known from approximation theory that the convergence of the related finite-element procedure requires smooth C^1-continuous shape functions. On unstructured meshes it is not possible to ensure strict slope continuity across finite elements when the elements are endowed with purely local polynomial shape functions and the nodal degrees of freedom consist of displacements and slopes only. Inclusion of higher derivatives among the nodal variables lead to several well known difficulties, e.g. spurious oscillations in the solution, non-physical higher order derivatives at the boundary vertices, or complex schemes for nonsingular parameterization of the derivatives for large

*cirak@cacr.caltech.edu
†rapa@mit.edu

rotations. These difficulties can be avoided by using *"non-local"* subdivision shape functions for the discretization of Kirchhoff-Love type shell theories on unstructured meshes. The displacement field within one finite element is interpolated through the displacements of the vertices attached to the element and the immediately adjacent vertices in the mesh. In the resulting shell discretization, the nodal displacements of the subdivision finite elements constitute the only unknowns of the shell problem.

In the following we give a brief summary of the assumed shell kinematics. A class of finite-deformation Kirchhoff-Love shell theories may be obtained from the ansatz:

$$\begin{aligned} \overline{\boldsymbol{\varphi}}(\theta^1,\theta^2,\theta^3) &= \overline{\boldsymbol{x}}(\theta^1,\theta^2)+\theta^3\overline{\boldsymbol{a}}_3(\theta^1,\theta^2) \qquad (1)\\ &\quad \text{with} \quad -\frac{\overline{h}}{2}\le\theta^3\le\frac{\overline{h}}{2}\\ \boldsymbol{\varphi}(\theta^1,\theta^2,\theta^3) &= \boldsymbol{x}(\theta^1,\theta^2)+\theta^3\boldsymbol{a}_3(\theta^1,\theta^2) \qquad (2)\\ &\quad \text{with} \quad -\frac{\overline{h}}{2}\le\theta^3\le\frac{\overline{h}}{2} \end{aligned}$$

where $\overline{\boldsymbol{\varphi}}(\theta^1,\theta^2,\theta^3)$ is the position vector of a material point associated with the convective coordinates $\{\theta^1,\theta^2,\theta^3\}$ within the shell body in its undeformed configuration. Similarly, $\boldsymbol{\varphi}(\theta^1,\theta^2,\theta^3)$ with respect to the deformed configuration of the shell. The pair $\{\theta^1,\theta^2\}$ defines a system of surface curvilinear coordinates, and the functions $\overline{\boldsymbol{x}}$ and $\boldsymbol{x}$ furnish a parametric representation of the undeformed and deformed shell middle surfaces, respectively. The thickness of the undeformed shell is $\overline{h}$ and the parameter θ^3 determines the position of a material point on the normal to the undeformed middle surface.

The unit normals to the undeformed and deformed shell middle surface are:

$$\overline{\boldsymbol{a}}_3=\frac{\overline{\boldsymbol{x}}_{,1}\times\overline{\boldsymbol{x}}_{,2}}{\overline{j}} \qquad \boldsymbol{a}_3=\frac{\boldsymbol{x}_{,1}\times\boldsymbol{x}_{,2}}{j} \qquad (3)$$

Here and henceforth comma is used to denote partial differentiation. With the aid of these kinematic assumptions, the deformation gradient $\boldsymbol{F}$ for the shell body may be expressed in the form:[9]

$$\boldsymbol{F}=\frac{\partial\boldsymbol{\varphi}}{\partial\overline{\boldsymbol{\varphi}}}=\frac{\partial\boldsymbol{\varphi}}{\partial\theta^i}\otimes\frac{\partial\theta^i}{\partial\overline{\boldsymbol{\varphi}}} \qquad (4)$$

In this derivation the summation convention is assumed to be in force.

The potential energy of the shell body takes the form

$$\Pi_{int}[\boldsymbol{\varphi}]=\int_{\overline{\Omega}}\int_{-\frac{\overline{h}}{2}}^{\frac{\overline{h}}{2}} W(\boldsymbol{F})\,\mu\,d\theta^3 d\overline{\Omega} \qquad (5)$$

where, for an elastic material, W is the strain-energy density per unit undeformed volume and

$$\mu=\frac{|(\overline{\boldsymbol{g}}_1\times\overline{\boldsymbol{g}}_2)\cdot\overline{\boldsymbol{g}}_3|}{|(\overline{\boldsymbol{a}}_1\times\overline{\boldsymbol{a}}_2)\cdot\overline{\boldsymbol{a}}_3|} \qquad (6)$$

accounts for the curvature of the shell in the computation of the element of volume. We consider a Neo-Hookean material extended to the compressible range.

$$W(\boldsymbol{C})=\frac{\lambda_0}{2}(\log J)^2-\mu_0\log J+\frac{\mu_0}{2}(\mathrm{tr}\boldsymbol{C}-3) \qquad (7)$$

where λ_0 and μ_0 are material parameters,

$$J=\det(\boldsymbol{F}) \qquad (8)$$

is the determinant of the deformation and

$$\boldsymbol{C}=\boldsymbol{F}^T\boldsymbol{F} \qquad (9)$$

is the right Cauchy-Green deformation tensor.

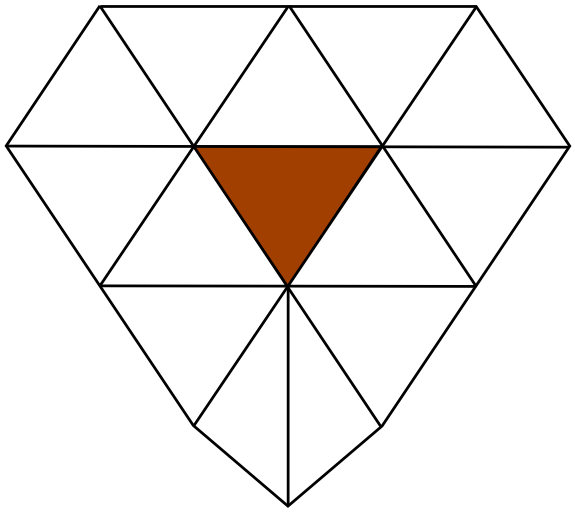

Fig. 1 Triangular element and its control nodes.

In our subdivision scheme based finite element method, the discretized shell surface is entirely determined by the vertex positions of the triangulation, or *control mesh*. This results in a particularly simple discretization of the undeformed and deformed shell surfaces within one finite element:[7]

$$\overline{\boldsymbol{x}}_h=\sum_{I=1}^{NP}N^I\overline{\boldsymbol{x}}_I \qquad \boldsymbol{x}_h=\sum_{I=1}^{NP}N^I\boldsymbol{x}_I \qquad (10)$$

where $\overline{\boldsymbol{x}}_I$ and $\boldsymbol{x}_I$ are the vertex coordinates, and NP is the number of the vertices in the one neighborhood of the element (Fig. 1). The subdivision method guarantees that all such element patches exactly match at their boundaries at least in C^1 sense. Introduction of the discretization into the weak form yields a semi-discrete system of equations of the form:

$$\boldsymbol{M}_h\ddot{\boldsymbol{x}}_h+\boldsymbol{f}_h^{int}(\boldsymbol{x}_h)=\boldsymbol{f}_h^{ext}(t) \qquad (11)$$

where $\boldsymbol{M}_h$ is the mass matrix, $\boldsymbol{f}_h^{int}(\boldsymbol{x}_h)$ is the internal force array, and $\boldsymbol{f}_h^{ext}(t)$ is the external force array.

The equations of motion are integrated in time with the explicit Newmark algorithm:

$$\begin{aligned} \boldsymbol{x}_{n+1} &= \boldsymbol{x}_n+\Delta t\dot{\boldsymbol{x}}_n+\frac{1}{2}\Delta t^2\ddot{\boldsymbol{x}}_n \qquad (12)\\ \dot{\boldsymbol{x}}_{pre} &= (1-\gamma)\Delta t\ddot{\boldsymbol{x}}_n+\dot{\boldsymbol{x}}_n \qquad (13) \end{aligned}$$

in which $\dot{\boldsymbol{x}}_{pre}$ are the predictor velocities and the final velocities follow from:

$$\begin{aligned} \ddot{\boldsymbol{x}}_{n+1} &= \boldsymbol{M}^{-1}(\boldsymbol{f}_n^{ext}-\boldsymbol{f}^{int}(\boldsymbol{x}_n) \qquad (14)\\ \dot{\boldsymbol{x}}_{n+1} &= \dot{\boldsymbol{x}}_{pre}+\gamma\Delta t\ddot{\boldsymbol{x}}_{n+1} \qquad (15) \end{aligned}$$

where γ is the Newmark damping parameter.

Eulerian Compressible Fluid Solver

In this section we summarize the details of the employed fluid solver[10,11] for the inviscid compressible flow:

$$\begin{aligned} \frac{\partial\rho}{\partial t}+\nabla\cdot(\rho\boldsymbol{u})&=0\\ \frac{\partial}{\partial t}(\rho\boldsymbol{u})+\nabla\cdot(\rho\boldsymbol{u}\otimes\boldsymbol{u}+\boldsymbol{I}p)&=0 \qquad (16)\\ \frac{\partial}{\partial t}(\rho E)+\nabla\cdot\left[\rho\boldsymbol{u}\left(E+\frac{p}{\rho}\right)\right]&=0 \end{aligned}$$

where ρ is the density, $\boldsymbol{u}$ is the velocity vector, p is the pressure, e is the specific internal energy, and $E=e+\frac{1}{2}\|\boldsymbol{u}\|^2$

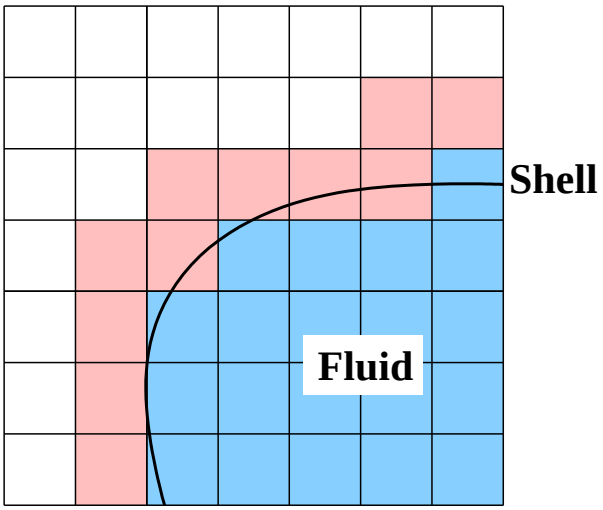

Fig. 2 Identification of the fluid and the ghost cells given the instant location of the shell

is the specific total energy. In the case of a perfect gas the equation of state takes the form:

$$p = (\gamma - 1)\rho e \tag{17}$$

in which γ is the specific heat ratio.

Our spatial discretization scheme corresponds to a finite volume formulation on a Cartesian grid. The spatially-discretized equations are integrated in time by recourse to the second-order Runge-Kutta algorithm. The fluxes at the cell interfaces may be calculated either by the Equilibrium Flux Method (EFM) (a kinetic flux vector splitting scheme),[12] or the Godunov or Roe method (a flux difference splitting scheme). Second order accuracy is achieved via linear reconstruction with Van Leer type slope limiting applied to projections in characteristic state space.[13] More details of this formulation and its parallel implementation including adaptive mesh refinement capability can be found in Ref.[14]

Eulerian-Lagrangian Fluid-Shell Coupling

A critical aspect of the proposed numerical strategy is to formulate a theoretically sound and computationally effective means of algorithmically coupling the Lagrangian shell and the Eulerian fluid solver. Towards this end, we extend the previous work on coupling compressible flows interacting with bulk solid materials.[5,14] We use a loosely-coupled explicit approach and apply appropriate interface boundary conditions at the beginning of each time step to both solvers. The interface boundary conditions for the solvers follow from explicitly enforcing the conservation laws at the interface.

In the fluid solver, the zero-mass-flux and free-tangential-flow (slip) boundary conditions, required for the inviscid Euler model, are enforced through properly populating the fluid velocities and two thermodynamic variables (pressure and density) in the so-called ghost cells, Fig.2. Ghost cells lie outside the physical fluid domain and their field variables are chosen so that the flow solver can be used without any further modifications. To that purpose, initially the velocity, pressure, and density cell averages in the active fluid domain are extrapolated to the adjacent inactive ghost cells. Subsequently, the ghost cell velocities are modified so that the fluid velocity normal to the interface is zero:

$$\boldsymbol{u}_F = \big[(2\boldsymbol{u}_S - \tilde{\boldsymbol{u}}_F)\cdot\boldsymbol{n}\big]\boldsymbol{n} + (\tilde{\boldsymbol{u}}_F\cdot\boldsymbol{t})\boldsymbol{t} \tag{18}$$

where $\tilde{\boldsymbol{u}}_F$ is the fluid velocity extrapolated from the active fluid cells and $\boldsymbol{u}_S$ is the shell velocity. The location of the fluid-shell interface, its normal $\boldsymbol{n}$, and its tangent $\boldsymbol{t}$ are obtained at each time step on the fluid grid by recourse to a level set function.[15]

The level set function $\phi(\boldsymbol{x})$ is the signed distance of the fluid-shell interface to the fluid cells. The location of the fluid-shell interface on the fluid grid is implicitly represented by the zeroth level set:

$$\phi(\boldsymbol{x}) = 0 \tag{19}$$

The sign of ϕ determines whether the fluid cell is interior, ($\phi < 0$), or exterior to the real fluid, ($0 \le \phi \le \phi_S$). A key ingredient for the success of the proposed coupling strategy is the optimal signed distance computation algorithm presented by Mauch.[6]

The interface boundary location and velocity are dictated by the Lagrangian shell solver. The level set information is used for a bilinear interpolation of the fluid cell pressures onto the deformed configuration of the shell. The momentum transfer from the fluid to the shell is effectively accomplished *via* a consistent integration of the fluid pressure as traction boundary conditions on the shell finite element mesh.

The proposed method avoids the robustness issues associated with cut-cell approaches–especially in three dimensions– and furnishes, in effect, a general coupling method for the interaction of high-speed flows with highly-deformable solids. The introduced algorithm's overall computational complexity is determined by the level set computation and is of order $O(m+n)$, where m is the number of grid points in the subset of the fluid grid where the level set is required and n is the number of elements in the shell mesh.

The resulting algorithms are implemented on the Virtual Test Facility for Simulating the Dynamic Response of Materials.[4] Details of its software architecture as well as of its implementation and scalability properties on large numbers of processors may be found in the cited reference.

Example

We consider the simulation of airbag deployment for demonstrating the feasibility and power of the developed method in computing the complex interactions of high speed flows with highly-deformable thin-shell structures.

The simulation corresponds to an initially-flat airbag made of an elastic fabric with a Young's Modulus of $E = 6.0\cdot 10^9 Pa$, Poisson's ratio of $\nu = 0.3$, and mass density of $\rho = 1000.0\frac{kg}{m^3}$. The thickness of the airbag is $7.3\cdot 10^{-4} m$ and the diameter in its flat initial configuration is $D = 0.74m$. The discretization of the airbag consists of 10176 subdivision thin-shell elements and 5101 vertices.

The gas enters the airbag with a pressure of $p = 12.0atm$, mass density of $\rho = 16.0\frac{kg}{m^3}$, and velocity of $u_z = 73.0\frac{m}{s}$. The initial properties of the gas are: $p = 1.0atm$, $\rho = 13.0\frac{kg}{m^3}$, and $\gamma = 1.4$. The expanding gas generates a weak shock wave that propagates inside the airbag and interacts with the airbag walls. The inlet conditions of the gas are kept constant until $9,71\mu s$ and later changed to reflecting type boundary conditions. The fluid domain of $0.86m \times 0.86m \times 0.49m$ is discretized with $48\times 48\times 62$ fluid cells.

Figures 3-6 show a sequence of snapshots of the simulation. The deformed airbag meshes are shown on the left of each figure and the pressure isocontours on the center-plane are shown on the right of each figure. The portions of the fluid grid that are external to the airbag have been left out for visual clarity by making use of the level set function one more time at postprocessing. Important features of the mechanics of the airbag deployment process can be observed in these figures, including the high-frequency wrinkling modes of the airbag fabric and the shock reflections of the gas on the deforming airbag walls. The ability of the presented method to capture these complex features of the coupled interaction between the flow and the airbag fabric is particularly noteworthy.

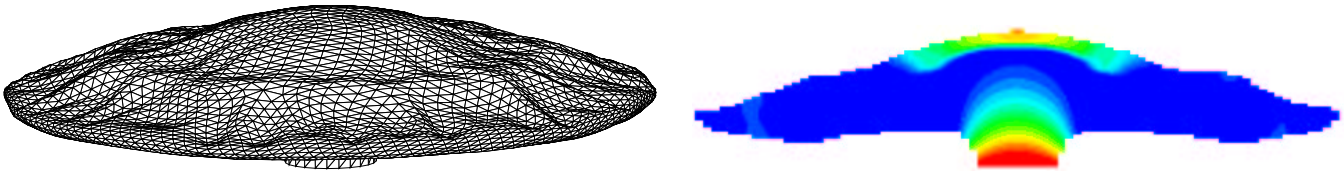

a) Deformed finite element mesh b) Slice of pressure isosurfaces in fluid

Fig. 3 Simulation of airbag deployment: Step 2500 after $4.25\mu s$

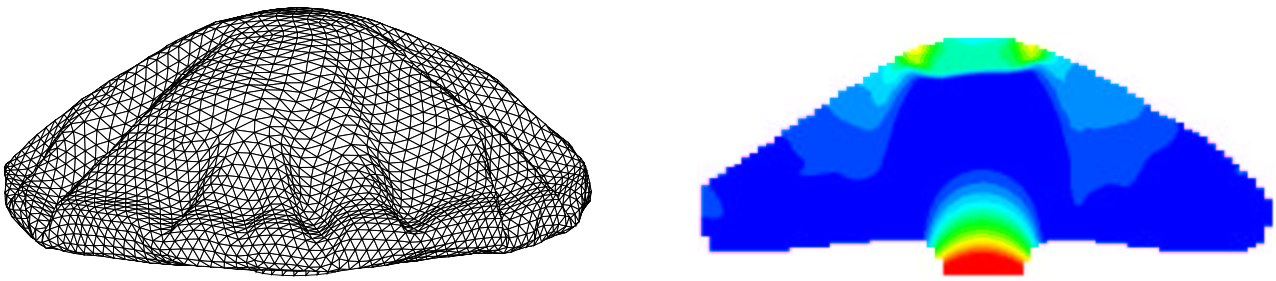

a) Deformed finite element mesh b) Slice of pressure isosurfaces in fluid

Fig. 4 Simulation of airbag deployment: Step 5000 after $8.16\mu s$

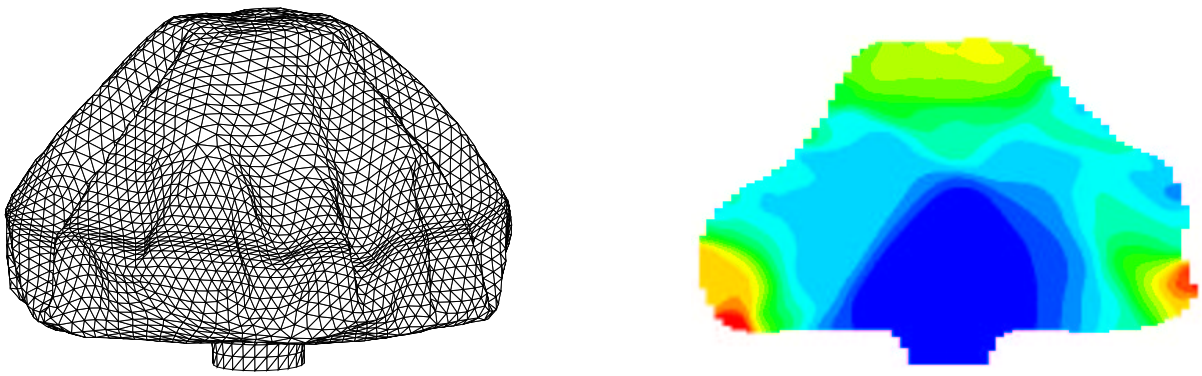

a) Deformed finite element mesh b) Slice of pressure isosurfaces in fluid

Fig. 5 Simulation of airbag deployment: Step 7500 after $12.13\mu s$

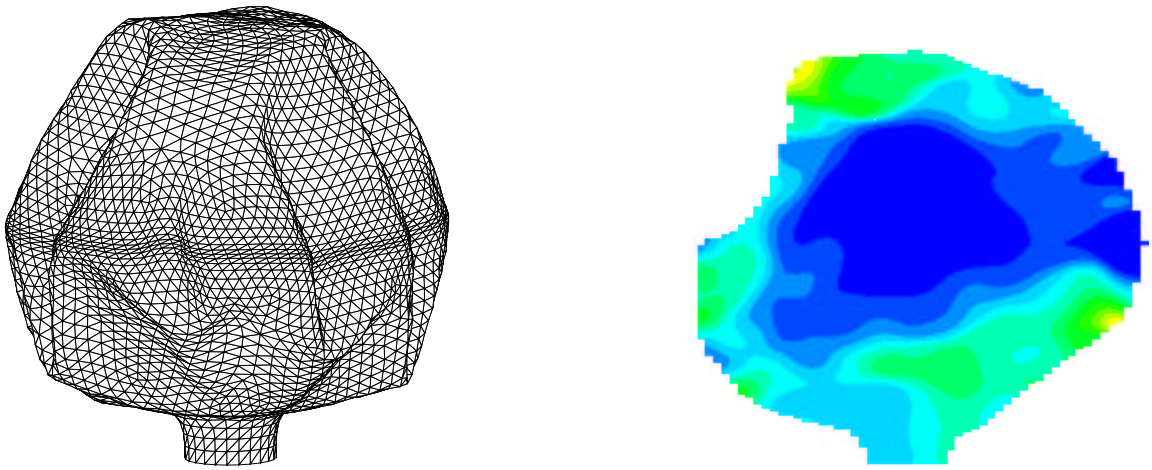

a) Deformed finite element mesh **b) Slice of pressure isosurfaces in fluid**

Fig. 6 Simulation of airbag deployment: Step 10000 after $18.02\mu s$

The simulations were performed using 58 Intel Pentium III processors on a Beowulf cluster with a one *Gbps* fast ethernet switch. The computation time for the whole simulation was approx. 15 hours.

Conclusions

We have developed a robust numerical approach for the simulation of compressible flows interacting with highly-deformable shells. The method furnishes an effective means of coupling Eulerian fluid solvers and Lagrangian large-deformation shell solvers, thus exploiting the power of these well established formulations in each component. We have demonstrated the efficiency and versatility of the proposed strategy in a simulation of an airbag deployment process. It bears emphasis that in the proposed approach both the solid and the fluid components, as well as their coupled interaction, are considered in full detail and modeled with an equivalent level of fidelity without any oversimplifying assumption or bias towards a particular physical aspect of the problem, as is common in most fluid-solid interaction approaches.

Acknowledgments

The partial support of DoE through Caltech's ASCI Center for the Simulation of the Dynamic Response of Materials is gratefully acknowledged. We are grateful to Michael Aivazis, Dan Meiron, and Julian Cummings from the Caltech ASCI Center for providing the Virtual Test Facility for Simulating the Dynamic Response of Materials. The algorithms presented in this work have been implemented on this computational framework.

References

[1] Radovitzky, R. and Ortiz, M., "Lagrangian finite element analysis of Newtonian fluid flows," *International Journal For Numerical Methods In Engineering*, Vol. 43, No. 4, 1998, pp. 607–617.

[2] Donea, J., "An arbitrary Lagrangian-Eulerian finite element method for transient fluid-structure interactions," *Computer Methods in Applied Mechanics and Engineering*, Vol. 33, 1982, pp. 689–723.

[3] Fedkiw, R., Aslam, T., Merriman, B., and Osher, S., "A Non-Oscillatory Eulerian Approach to Interfaces in Multimaterial Flows (The Ghost Fluid Method)," *J. Comput. Physics*, Vol. 152, 1999, pp. 457–492.

[4] Cummings, J., Aivazis, M., Samtaney, R., Radovitzky, R., Mauch, S., and Meiron, D., "A virtual test facility for the simulation of dynamic response in materials," *Journal Of Supercomputing*, Vol. 23, No. 1, 2002, pp. 39–50.

[5] Meiron, D., Radovitzky, R., and Samtaney, R., "The Virtual Test Facility: An Environment For Simulating The Nonlinear Dynamic Response Of Solids Under Shock And Detonation Wave Loading," *Proceedings of the Sixth U.S. National Congress on Computational Mechanics*, U.S. Association for Computational Mechanics, Dearborn, MI, 2001.

[6] Mauch, S., "A Fast Algorithm for Computing the Closest Point and Distance Transform," *Preprint, http://www.acm.caltech.edu/~seanm/software/cpt/cpt.html*, 2001.

[7] Cirak, F. and Ortiz, M., "Fully C^1-Conforming Subdivision Elements for Finite Deformation Thin-Shell Analysis," *Internat. J. Numer. Methods Engrg.*, Vol. 51, 2001, pp. 813–833.

[8] Cirak, F., Ortiz, M., and Schröder, P., "Subdivision Surfaces: A New Paradigm for Thin-Shell Finite-Element Analysis," *Internat. J. Numer. Methods Engrg.*, Vol. 47, No. 12, 2000, pp. 2039–2072.

[9] Marsden, J. E. and Hughes, T. J. R., *Mathematical foundations of elasticity*, Prentice-Hall, Englewood Cliffs, N.J., 1983.

[10] Samtaney, R. and Zabusky, N. J., "Circulation deposition on shock-accelerated planar and curved density-stratified interfaces: models and scaling laws," *J. Fluid Mech.*, Vol. 269, 1994, pp. 45–78.

[11] Samtaney, R. and Meiron, D. I., "Hypervelocity Richtmyer-Meshkov instability," *Phys. Fluids*, Vol. 9, No. 6, 1997, pp. 1783–1803.

[12] Pullin, D. I., "Direct simulation methods for compressible ideal gas flow." *J. Comput. Phys.*, Vol. 34, 1980, pp. 231–244.

[13] LevVeque, R. J., *Finite Volume Methods for Hyperbolic Problems*, Cambridge University Press, 2002.

[14] "ASCI Alliance Center for the Simulation of Dynamic Response of Materials, FY00 Annual Report," URL: http://www.cacr.caltech.edu/ ASAP/onlineresources/publications/, 2000.

[15] Sethian, J., *Level Set Methods and Fast Marching Methods*, Cambridge University Press, 1999.